Digital Intelligence PRESS
International Scientific Technical and Economic Research
https://doi.org/10.67541/istaer2625
Research Article Volume 4, Issue 3 (July 2026) Open Access

Research on Sintering End Temperature Control Based on Fuzzy Adaptive PID Control

Yunkai He[1,2,3] *, Jinfeng Yang[4]

[1] *School of Electrical and Automation Engineering, Nanjing Normal University, Nanjing, Jiangsu, China*
[2] *Jiangsu Provincial Key Laboratory of Three-dimensional Printing Equipment and Manufacturing, Nanjing Normal University, Nanjing, Jiangsu, China*
[3] *Jiangsu Kunlun Internet New Energy Group Co., Ltd., Nanjing, Jiangsu, China*
[4] *School of Electronics and Information Engineering, Nanchang Normal College of Applied Technology, Jiujiang, Jiangxi, China*

***Corresponding author:** Yunkai He. Email: yk2329156525@163.com

Abstract

The sintering end temperature serves as a critical process parameter for assessing the completion degree of the sintering process. Its control system exhibits significant inertia and pure delay characteristics, making conventional PID controllers struggle to maintain optimal performance under all operating conditions due to fixed parameters. This paper proposes a fuzzy adaptive PID control strategy that only adjusts proportional gain and derivative gain online while maintaining constant integral gain. Using the sintering end temperature as the controlled variable, performance comparisons were conducted with both a conventional PID controller tuned using Ziegler-Nichols method and the proposed approach regarding nominal tracking accuracy, output disturbance suppression capability, and model mismatch robustness. Results demonstrate that the proposed method reduces regulation time by 76.8% under nominal conditions without steady-state error; achieves maximum temperature deviation of merely 17.7% compared to conventional PID when subjected to a 25°C external disturbance; and maintains steady-state error within 0.5°C even under severe mismatch conditions where time constants and pure delay values increase by 33% and 37.5%, respectively. With its simple structure and strong robustness, this method provides an effective reference for field-based control of sintering end temperatures.

Keywords

Sintering end temperature; Fuzzy adaptive PID; Ziegler-Nichols; Robustness; Dynamic performance

Received: 16 Jul 2026; Revised: 20 Jul 2026; Accepted: 28 Jul 2026; Published: 30 Jul 2026

1. INTRODUCTION

Sintering is a critical thermal treatment process in metallurgical and advanced materials manufacturing where precise temperature control governs product quality, energy efficiency, and operational stability. In the iron and steel industry, the Burn-Through Point (BTP) temperature serves as the key completion indicator, yet its regulation through trolley speed is challenged by severe inertia, pure time delays, and nonlinearities. Beyond ferrous metallurgy, sintering temperature dictates the microstructure and properties of ceramics, battery materials, and alloys. For example, sintering temperature and carbon content determine the porosity and catalytic activity of polymer-derived SiOC ceramics, strict control during HET thin-layer construction is essential for pavement durability, microwave sintering of lithium aluminate ceramics achieves dense functional ceramics, blast furnace ferronickel slag can be converted into thermal insulation materials by precisely controlling temperature between 1000 °C and 1200 °C, temperature control during Spark Plasma Sintering is critical for up-scaling and complex shaping, and the thermal diffusivity of density-controlled sintered SiC links sintering conditions to thermal transport properties[1],[2],[3],[4],[5],[6]. These cross-domain demands motivate robust, adaptive control strategies.

Various control approaches have been explored, from classical PID enhancements to intelligent and data-driven methods. Intelligent systems using spatial–temporal graph convolutional networks, fuzzy logic optimized with ANFIS, LSTM-PID combinations, expert-experience-based PLC control, improved grey wolf optimiser with RBF neural network, and model predictive control for cathode material sintering have been applied to handle process complexities [7],[8],[9],[10],[11],[12]. Simultaneously, material-focused studies have related sintering temperature to corrosion resistance in magnesium alloys, microwave dielectric properties in ceramics, densification behaviour in ceramic cores, and secondary sintering of dedusting ash [13],[14],[15],[16]. Nevertheless, many intelligent controllers either rely on full three-parameter adaptation risking windup, or lack systematic comparison under disturbances and model mismatches. Advanced optimal control schemes, while theoretically appealing, impose heavy computational demands unsuitable for industrial controllers with limited online update capabilities.

To fill this gap, this paper proposes a fuzzy adaptive PID controller that adjusts only K_p and K_d online, keeping K_i constant, and systematically compares its performance against a conventional Ziegler–Nichols PID under three typical scenarios. Simulations demonstrate 76.8% reduction in settling time, superior disturbance suppression (24.98 °C maximum deviation versus 141.03 °C), and robust steady-state error below 0.5 °C even under 33% and 37.5% increases in time constant and delay, providing a practically viable reference for sintering temperature control.

2. SINTERING END TEMPERATURE MODEL

The sintering end temperature (Burn-Through Point, BTP) is controlled by adjusting the trolley speed; this process exhibits significant inertia and pure delay characteristics. Increasing the trolley speed shortens the heating time of the material layer and lowers the end temperature, demonstrating an inverse relationship between the two. When linearized near specific operating conditions, the behavior can be approximated as a first-order inertial plus pure delay model. Using the nominal parameters—static gain $K = 15$, time constant $T = 150$ s, and pure delay $\tau = 80$ s—the transfer function is derived as follows:

$$G(s) = \frac{K}{Ts+1}e^{-\tau s} = \frac{15}{150s+1}e^{-80s} \tag{1}$$

This model effectively captures the dominant dynamic characteristics of the controlled object and has been widely adopted in relevant studies [17],[18].

For digital simulation, a sampling period $T_s = 1$ s was selected, and the first-order inertial component was discretized using the zero-order hold method, yielding:

$$\mathrm{G(z)} = \frac{\mathrm{b_0 z^{-1}}}{1 + \mathrm{a_1 z^{-1}}} \tag{2}$$

Where: $\mathrm{a_1} = -\mathrm{e}^{-\mathrm{T_s/T}} \approx -0.9934, \mathrm{b_0} = \mathrm{K}(1 - \mathrm{e}^{-\mathrm{T_s/T}}) \approx 0.0997.$

The pure lag corresponds to $d = \tau/T_s = 80$ step delays. The system difference equation is:

$$y(k) = -a_1 y(k-1) + b_0 u(k-d-1) \tag{3}$$

Here u represents the trolley speed deviation and y the terminal temperature deviation. The simulation sets the target temperature to 450 °C ± 40 °C and the duration to 4000 s. This model will be used for subsequent controller design and closed-loop simulation.

3. CONTROLLER DESIGN

3.1 Conventional PID controller tuned via Ziegler-Nichols method

A conventional PID controller uses the deviation $e(k)$ between the set sintering end temperature and the actual output as input, and calculates the control variable $u(k)$ in real time using the discretized equation:

$$u(k) = K_p e(k) + K_i \sum_{j=0}^{k} e(j) T_s + K_d \frac{e(k) - e(k-1)}{T_s} \tag{4}$$

In the formula, $T_s = 1$ s is the system sampling period; K_p, K_i, and K_d represent the proportional gain, integral gain, and derivative gain, respectively. To limit the output range of the trolley speed actuator, the control signal output limit is set to $[-40,40]$ [19],[20].

For a typical first-order inertial-plus-pure-delay controlled object model $G(s) = \frac{K}{Ts+1} e^{-\tau s}$ in the sintering process, the Ziegler-Nichols open-loop step-response method was employed for parameter tuning, with the following tuning rules [21]:

$$K_p = \frac{1.2T}{K\tau}, T_i = 2\tau, T_d = 0.5\tau \tag{5}$$

Substituting the object characteristics $\mathrm{K} = 15$, $\mathrm{T} = 150$ s, and $\tau = 80$ s yields the fundamental tuning parameters: $\mathrm{K_p} \approx 0.15$, integral time constant $\mathrm{T_i} = 160$ s, and derivative time constant $T_d = 40$ s. Further conversion gives the discrete gains: $K_i = K_p/T_i \approx 0.00094$, and $K_d = K_p \cdot T_d \approx 6.0$.

This simulation experiment adopts fixed ZN-PID parameters: $K_p = 0.50$, $K_i = 0.001$, $K_d = 3.0$.

3.2 Fuzzy adaptive PID controller

3.2.1 Controller structure

The fuzzy adaptive PID controller designed in this paper is composed of two series-connected modules: a fuzzy inference module and a PID calculation module, as shown in Figure 1.

The fuzzy inference module takes system error e and error change rate ec as inputs, and outputs real-time correction terms of proportional gain ΔK_p and derivative gain ΔK_d. The PID module completes control computation with updated parameters, while the integral gain K_i remains constant throughout the whole process [22],[23].

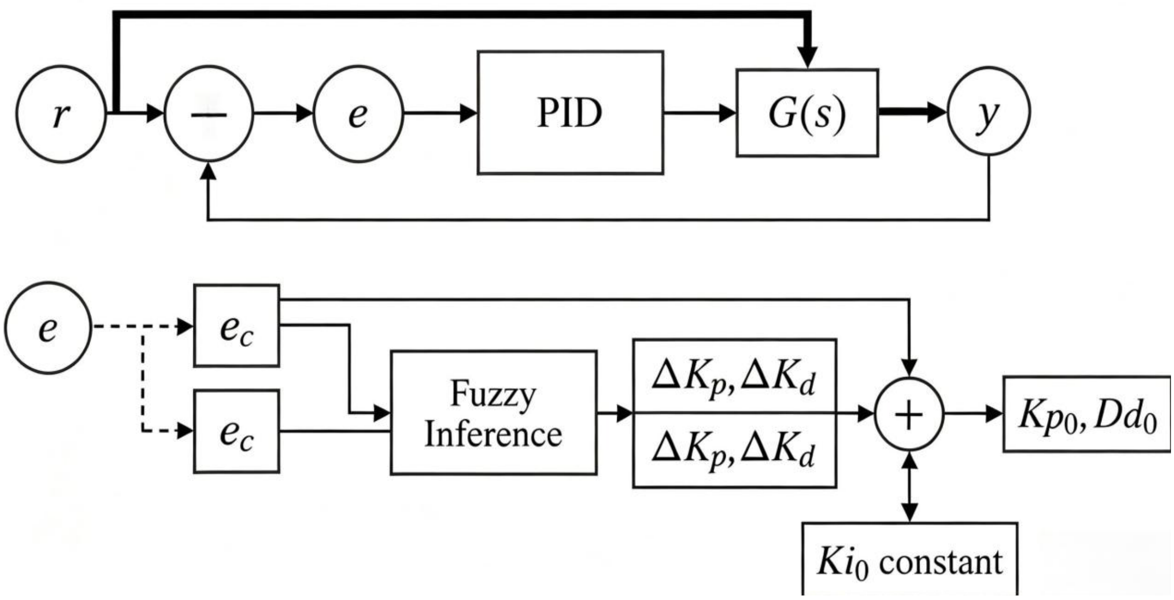

Figure 1. Block diagram of the fuzzy adaptive PID controller structure

The integral parameter is free from online adaptive adjustment. This design eliminates steady-state error of the system, and simultaneously avoids integral saturation, high-frequency oscillation and other defects induced by continuous dynamic adjustment of parameters.

3.2.2 Fuzzification and membership function design

Input variables e, ec and output correction terms ΔK_p, ΔK_d of the fuzzy inference system are uniformly normalized to the unified domain $[-1,1]$. All variables are divided into seven symmetric triangular fuzzy subsets: NB (Negative Big), NM (Negative Medium), NS (Negative Small), ZO (Zero), PS (Positive Small), PM (Positive Medium), PB (Positive Big) [24]. The corresponding membership function curves are displayed in Figure 2.

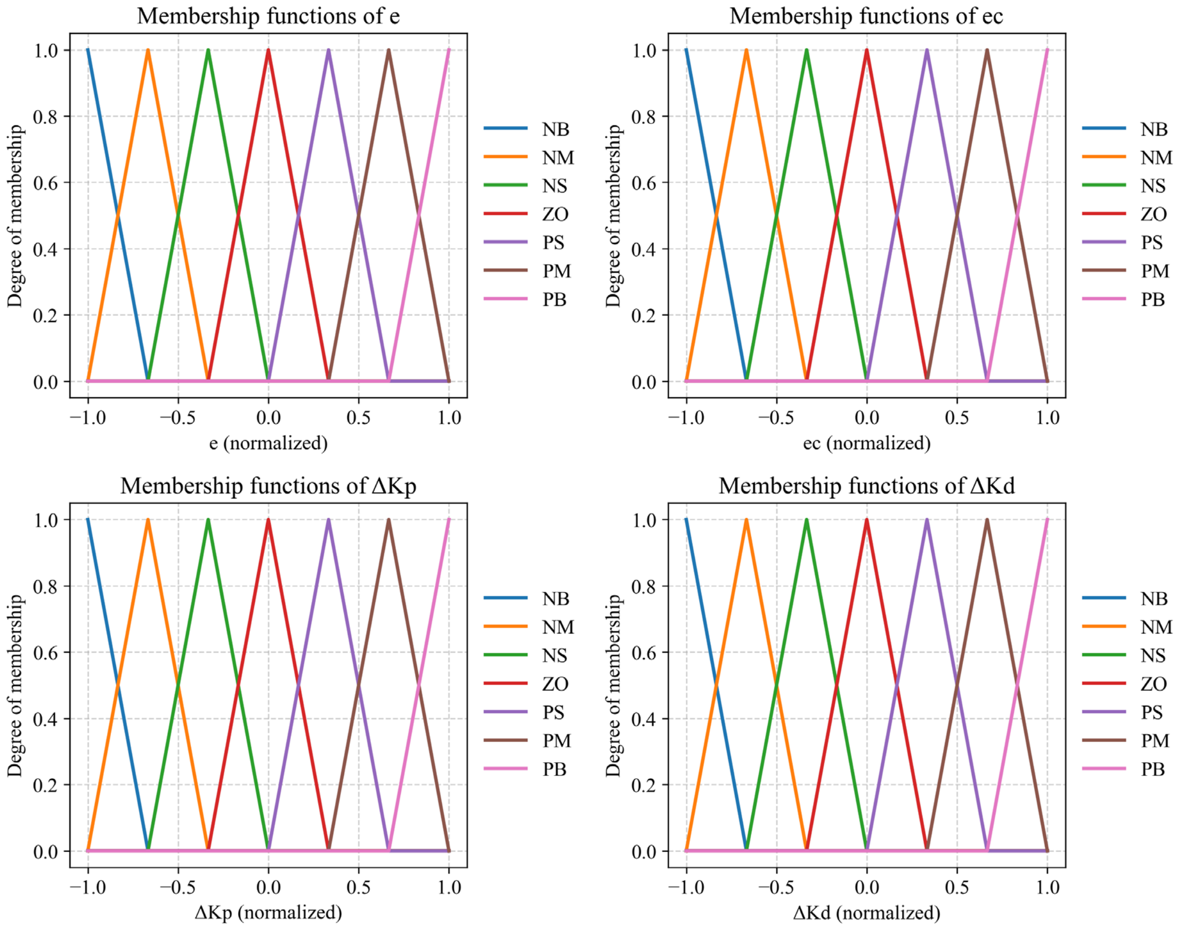

Figure 2. Curves of membership functions for input/output variables

Physical variables are mapped to normalized domain via quantization factors and scaling factors, whose specific values are listed as follows:

Error quantization factor $K_e = 1/30$, corresponding to actual temperature error range ±30 °C;

Error change rate quantization factor $K_{ec} = 1/3$, corresponding to temperature error change rate range ±3 °C/s;

Output correction scaling factors: $K_{\Delta K_p} = 0.03$, $K_{\Delta K_d} = 0.2$.

Benchmark PID parameters: $K_{p0} = 0.08$, $K_{d0} = 0.3$, fixed integral gain $K_{i0} = 0.0008$. Under this setting, the proportional gain varies smoothly within 0.05–0.11, and the derivative gain is slightly adjusted in the range of 0.1–0.5. Parameters change mildly without triggering system oscillation.

3.2.3 Fuzzy control rules

The core design idea of fuzzy rules is summarized as follows: when the system error is large, increase ΔK_p to accelerate response speed; when the error is small but its change rate is large, properly reduce ΔK_p and raise ΔK_d to restrain overshoot and sustained oscillation. Based on the above principle, a 7×7 two-dimensional fuzzy rule table is established (Table 1), where each cell stores corresponding linguistic fuzzy values.

Table 1. Fuzzy control rule table ($\Delta K_p/\Delta K_d$)

e\ec	NB	NM	NS	ZO	PS	PM	PB
NB	PB/PS	PB/PS	PM/ZO	PM/ZO	PS/ZO	ZO/PM	ZO/PB
NM	PB/NS	PB/NS	PM/NS	PS/NS	PS/ZO	ZO/PS	NS/PM
NS	PM/NB	PM/NM	PS/NS	PS/NS	ZO/ZO	NS/PS	NS/PM
ZO	PM/NB	PS/NM	PS/NS	ZO/NS	NS/ZO	NM/PS	NM/PM
PS	PS/NB	PS/NM	ZO/NM	NS/NS	NS/ZO	NM/PS	NM/PM
PM	PS/PM	ZO/NS	NS/NS	NM/NS	NM/ZO	NB/PS	NB/PB
PB	ZO/PB	NS/PM	NM/PM	NM/PS	NB/ZO	NB/PS	NB/PB

The Mamdani fuzzy reasoning method is adopted for rule operation in this work. Take the first rule in the table as an example, its logical expression is:

$$\frac{\text{IF e is NB AND ec is NB}}{\text{THEN } \Delta \mathrm{K_p} \text{ is PB AND } \Delta \mathrm{K_d} \text{ is PS}} \tag{7}$$

3.2.4 Online parameter updating and fuzzy output surface

In each sampling cycle, the fuzzy inference unit first quantifies the collected error e and error change rate ec, calculates normalized correction increments $\Delta K_p(k)$ and $\Delta K_d(k)$; then converts them into actual correction values by output scaling factors, and updates real-time proportional gain K_p and derivative gain K_d [25]. The updating formulas are given by:

$$K_p(k) = K_{p0} + K_{\Delta K_p} \cdot \Delta K_p(k), K_d(k) = K_{d0} + K_{\Delta K_d} \cdot \Delta K_d(k) \tag{8}$$

The integral gain remains constant as $K_i(k) = K_{i0}$ all the time. Substitute updated $K_p(k)$, fixed K_{i0} and $K_d(k)$ into Equation (5) to obtain the controller output at current sampling moment.

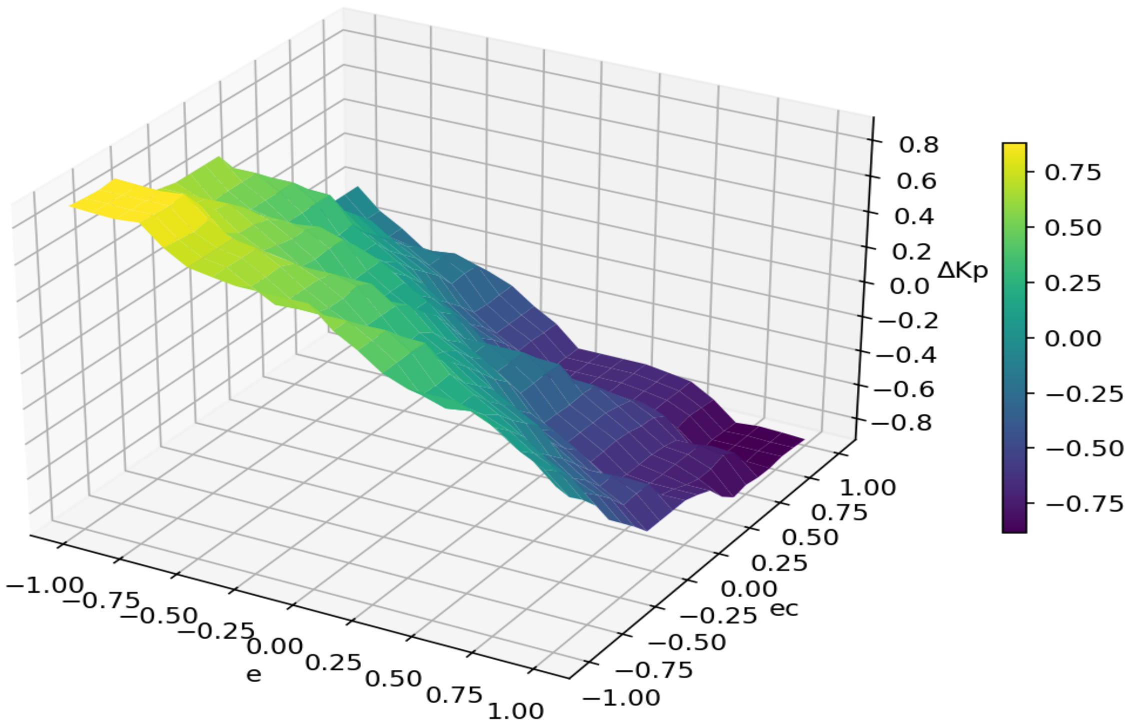

Figure 3. Fuzzy ΔK_p output surface

To intuitively reflect the nonlinear regulation characteristic of fuzzy inference, Figure 3. draws the 3D output surface of ΔK_p varying with error e and error change rate ec. The surface distribution conforms to control design logic: when both error and error change rate are PB, ΔK_p turns to NB, which automatically decreases proportional gain to suppress overshoot; when error is NB, ΔK_p becomes PB to strengthen control action rapidly and eliminate large deviation. It realizes the control target of "fast regulation for large deviation and stable convergence to set value".

4. SIMULATION EXPERIMENTS AND RESULT ANALYSIS

4.1 Simulation settings

To comprehensively compare the control performance of the ZN-PID controller and the fuzzy adaptive PID controller, three sets of closed-loop simulation experiments—step-response tracking under the nominal model, disturbance rejection under steady-state conditions with a sudden output perturbation, and robustness verification under model parameter perturbations—were conducted on the MATLAB/Simulink platform using the first-order plus dead-time model of the sintering end-point temperature established in Chapter 2 (model parameters: gain $K = 15$, time constant $T = 150\ s$, dead time $\tau = 80\ s$, with a uniform simulation setup of a total duration of $4000\ s$, a sampling period of $1\ s$, and a temperature setpoint of 450°C; the quantitative evaluation indices cover dynamic and steady-state performance (overshootσ, settling time t_s within a $\pm 2\%$ error band, and steady-state error e_{ss}) as well as disturbance rejection capability (maximum dynamic deviation $\Delta y_{\max}$ and recovery time t_{rec}).

4.2 Step response under nominal operating conditions

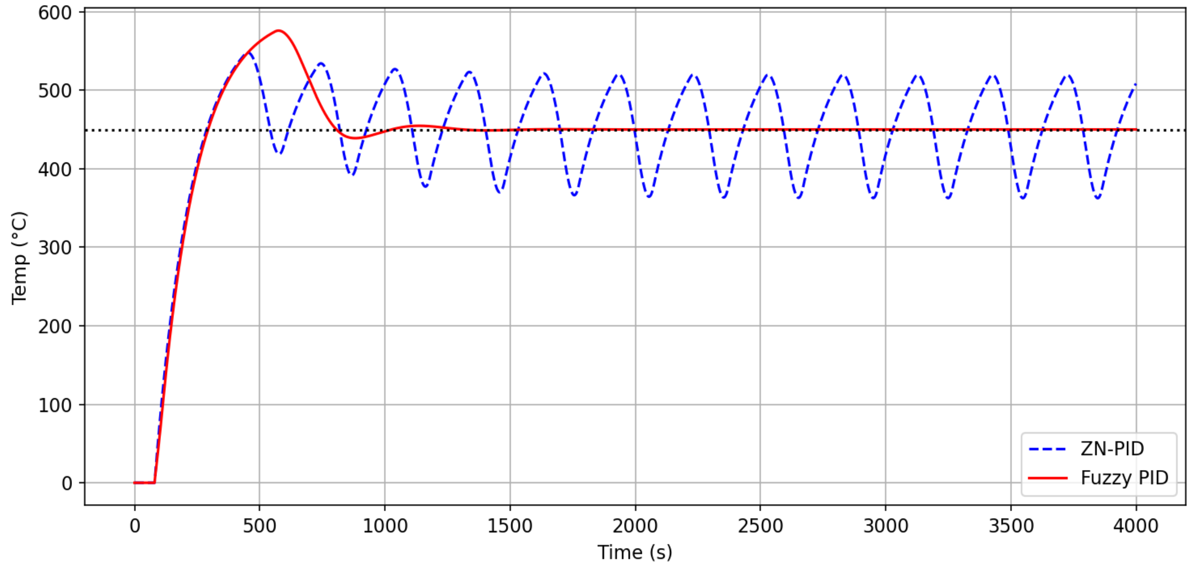

Figure 4. Step response curve under nominal operating conditions

Even at the simulation cutoff time (4000 s), the system fails to enter a steady-state region; the regulation time is recorded as 3999s, with persistent steady-state error observed.

Table 2. Comparison of performance under nominal operating conditions

Metric	ZN-PID	Fuzzy adaptive PID
Overshoot σ/%	21.7	28.0
Settling time t_s/ s	3999	928
Steady-state error e_{ss}/ °C	0.26	0.00

The analysis of the curve in Figure 4 and the quantitative data in Table 2 shows that the overshoot of the ZN-PID controller is slightly lower (21.7%), but its setpoint gain ± 20.26,° Cis excessively aggressive, causing sustained oscillations of constant amplitude throughout the entire system operation. Even at the simulation cutoff time (4000 s), the system fails to enter a steady-state region; the regulation time is recorded as 3999s, with persistent steady-state error observed.

The fuzzy adaptive PID achieves a peak overshoot of 28% during the initial step phase, yet converges smoothly to the target temperature in just 928 seconds with zero steady-state error. This is primarily due to the fuzzy inference mechanism's ability to dynamically reduce the proportional gain and enhance differential damping when output approaches the setpoint, effectively suppressing subsequent sustained oscillations. By balancing dynamic responsiveness and steady-state stability, the fuzzy adaptive PID outperforms the fixed-parameter ZN-PID significantly in overall control performance.

4.3 Noise immunity performance

At the 2500th second of the simulation, a step-amplitude $+25$, °Cdisturbance was applied at the system output to simulate transient measurement jump disturbances in sintering exhaust gas temperature.

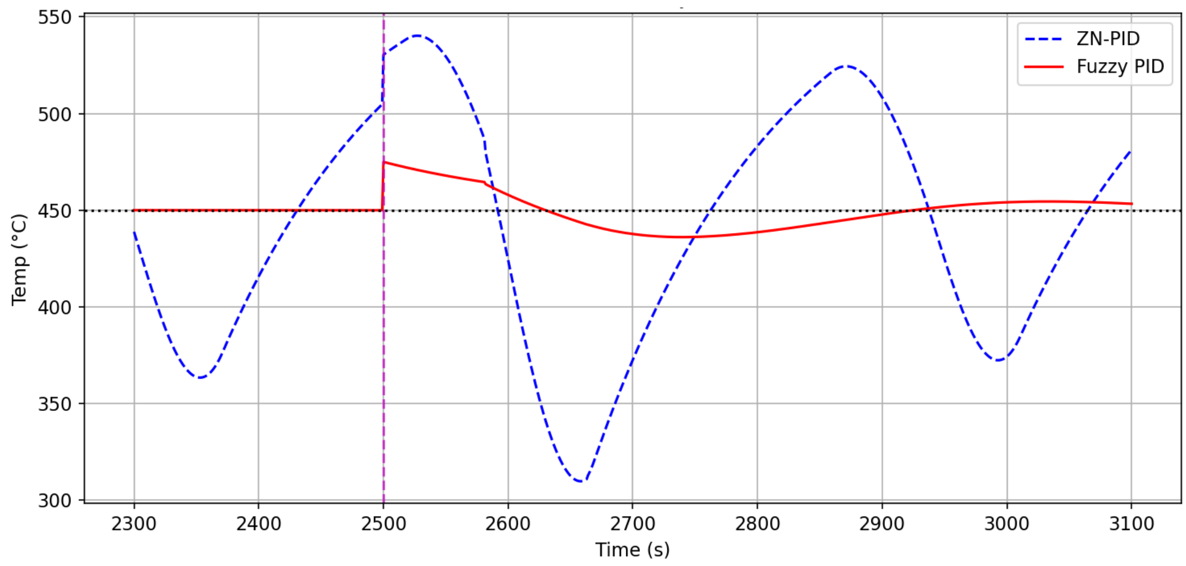

Figure 5. Localized magnified curve of disturbance conditions (2300–3100 s)

The output response curves of the two controllers are shown in Figure 5, while the quantified disturbance resistance metrics are presented in Table 3.

Table 3. Comparison of anti-interference performance

Metric	ZN-PID	Fuzzy adaptive PID
Maximum deviation Δy_{max}/ °C	141.03	24.98
Recovery time / t_{rec}	89	97

As shown in Table 3, under the same external disturbance, the maximum temperature deviation of ZN-PID reaches 141.03 °C (about 5.6 times the disturbance magnitude), and it still requires 89 s of oscillation attenuation to return to the steady state after the disturbance is removed. In contrast, the fuzzy adaptive PID shows a much smaller maximum deviation of only 24.98°C, and its recovery process is smooth without secondary oscillations. This difference arises because, with the nominal parameters, ZN-PID operates near the critical stability boundary, where external disturbances can easily trigger large sustained oscillations; the fuzzy adaptive PID, however, adjusts its parameters online in real time, increases system damping, and effectively suppresses output-side disturbances.

4.4 Robustness of the model parameters under perturbations

During actual sintering operations, real-time variations in material layer thickness and sinter permeability cause the object time constant $T = 200s$ and pure lag parameter $\tau = 110s$ to deviate from their nominal values. To verify the controller's robustness, the model parameters were adjusted; both controllers retained the original control parameters calibrated under nominal operating conditions.

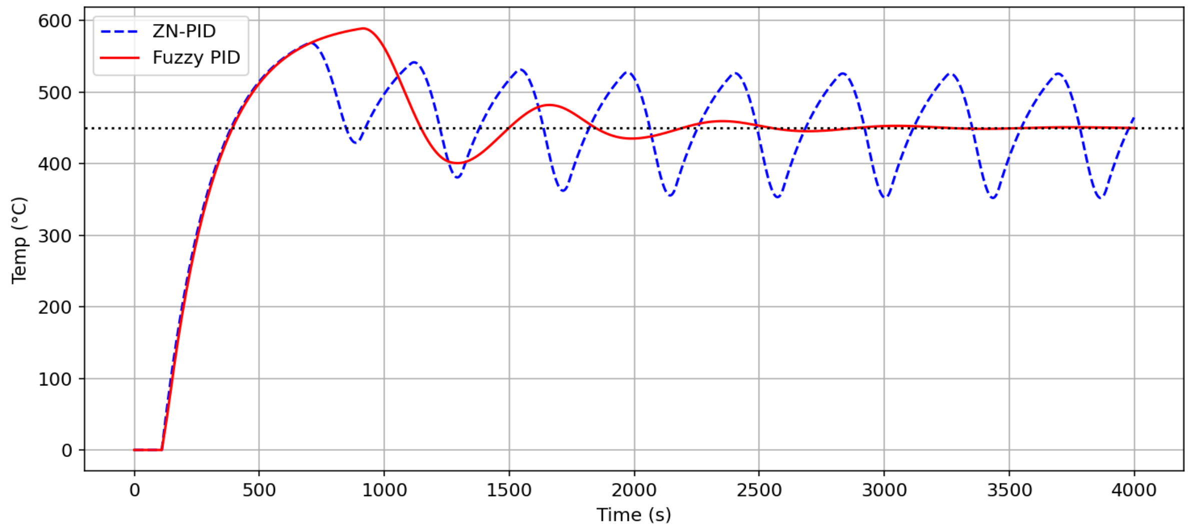

Figure 6. Step response curve under model perturbation

The step-response curves and performance metrics are shown in Figure 6 and Table 4, respectively.

Table 4. Performance comparison under model perturbations

Metric	ZN-PID	Fuzzy adaptive PID
Overshoot σ/%	32.9	30.7
Adjustment t_sTime / s	3999	2110
Steady-state e_{ss}error / °C	22.02	0.43

After model mismatch, the overshoot of ZN-PID increased to 32.9%, accompanied by a large steady-state error of 22.02 °C and persistent oscillations throughout the process, which completely failed to meet the requirements of sintering end-point temperature control. In contrast, the overshoot of the fuzzy adaptive PID rose only slightly to 30.7%, with a settling time of 2110 s and a very small steady-state error, showing much less performance degradation than ZN-PID. This is because fuzzy control does not rely on an accurate mathematical model of the plant; instead, it dynamically adjusts the control parameters based solely on the real-time error and its rate of change, thereby maintaining satisfactory dynamic and steady-state performance even under significant parameter variations and exhibiting outstanding robustness.

4.5 Analysis of the fuzzy adaptive mechanism

To elucidate the underlying mechanisms behind the performance differences between the two types of controllers, Figure 7. shows the controller output response curves under nominal operating conditions.

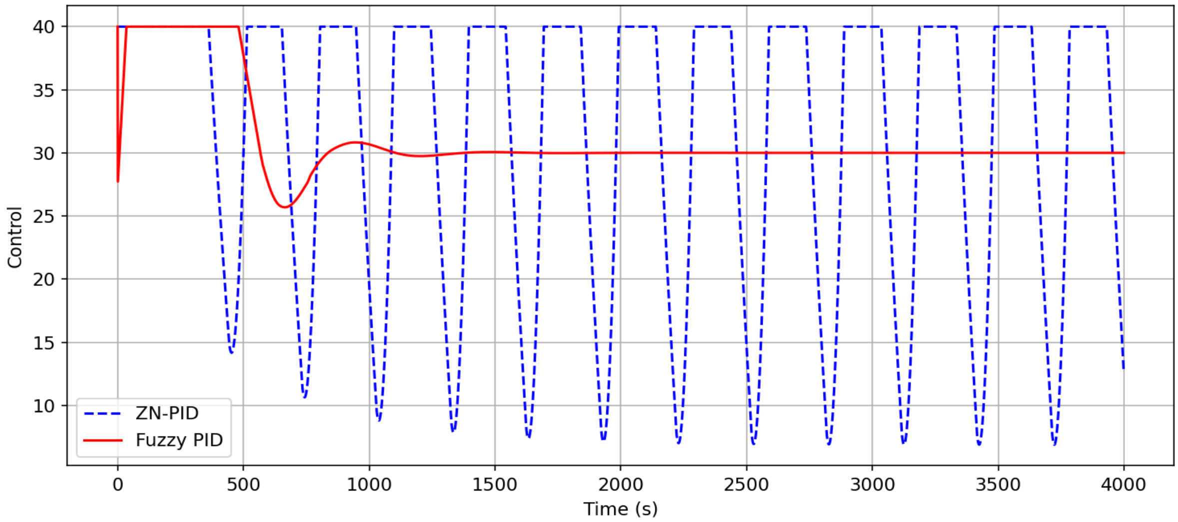

Figure 7. Comparison of control signals under nominal operating conditions

The control quantity curve in Figure 7. shows that the ZN-PID control signal enters a saturation region during the initial response phase, exhibiting frequent alternating positive and negative values throughout—directly causing sustained oscillations in system output. In contrast, the fuzzy adaptive PID controller flexibly adjusts its output based on the system's dynamic state, rapidly stabilizing to a constant minimum value after approaching steady-state, thereby preventing ineffective control-induced energy fluctuations.

5. CONCLUSION

This study addresses the large inertia and pure lag characteristics of sintering end temperature by developing a first-order inertial-plus-pure-lag model, and subsequently designing both a ZN-PID controller and a fuzzy adaptive PID controller that only adjusts the parameters (K_p and K_d) online.

The results demonstrate that the fuzzy adaptive PID achieves a settling time of merely 928 seconds under nominal conditions, 76.8% shorter than that of the ZN-PID, and exhibits no steady-state error; when subjected to an external disturbance of 25 °C, the maximum temperature deviation is only 24.98 °C, significantly lower than the 141.03 °C observed with ZN-PID; even under severe model mismatch conditions where the time constant and pure lag are increased by 33% and 37.5%, respectively, it maintains a steady-state error below 0.5 °C and excellent dynamic performance, showcasing remarkable robustness.

The proposed control strategy features a simple structure and easy engineering implementation, as it only requires online adjustment of two parameters (K_p and K_d) while keeping the integral gain constant, thereby avoiding integral windup and reducing computational overhead. This lightweight design can be readily deployed on standard industrial controllers such as PLCs or DCS without demanding high-performance computing resources or extensive model identification. The comprehensive simulation results across nominal, disturbed, and model mismatched conditions provide clear and practical guidance for commissioning and tuning in real sintering plants, confirming that the method can effectively overcome the process’s inherent large inertia and delay with minimal engineering effort.

Abbreviations

BTP, Burn-Through Point;

PID, Proportional-Integral-Derivative;

ZN-PID, Ziegler-Nichols PID;

FOPDT, First-Order Plus Dead-Time;

ADP, Adaptive Dynamic Programming;

MPC, Model Predictive Control;

RBF, Radial Basis Function;

ANFIS, Adaptive Neuro-Fuzzy Inference System;

LSTM, Long Short-Term Memory;

PLC, Programmable Logic Controller;

ST-ADP, Self-Triggered Adaptive Dynamic Programming;

MATLAB, Matrix Laboratory;

Simulink, Simulation and Link.

Supplementary Material

Not applicable.

Appendix

Not applicable.

Ethics approval and consent to participate.

This study did not involve human participants, animal subjects, or any data requiring ethical approval. Therefore, ethics approval and consent to participate are not applicable.

Acknowledgements

The authors would like to thank the editors of this journal and all the anonymous reviewers who provided valuable comments on this work.

Competing interests

The authors declare that they have no financial or personal relationships that may have inappropriately influenced them in writing this article.

Author contributions

All authors have read and agreed to the published version of the manuscript. The author's contributions are specified as follows: **Y.H.:** Conceptualization, Methodology, Software, Validation, Formal analysis, Investigation, Data Curation, Writing – Original draft, Writing – Review & Editing, Visualization, Supervision, Project administration. **J.Y.:** Conceptualization, Methodology, Validation, Formal analysis, Investigation, Writing - Original Draft, Writing - Review & Editing, Visualization.

Funding information

The authors declare that no funds, grants, or other support were received during the preparation of this manuscript.

Data availability

The data that support the findings of this study are available upon request from the corresponding authors, **Y.H.**

Disclaimer

The views and opinions expressed in this article are those of the authors and are the product of professional research. It does not necessarily reflect the official policy or position of any affiliated institution, funder, agency, or that of the publisher. The authors are responsible for this article's results, findings, and content.

Declaration of AI and AI-assisted Technologies in the Writing Process

During the writing of this article, the author used ChatGPT for spelling and grammar checking. After using this tool, the author reviewed and edited the content as needed and assumes full responsibility for the final published content.

REFERENCES

[1] Solodkyi, I., Bogomol, I., & Loboda, P. (2022). High-speed electron beam sintering of WC-8Co under controlled temperature conditions. *International Journal of Refractory Metals and Hard Materials*, *102*, 105730. https://doi.org/10.1016/j.ijrmhm.2021.105730

[2] Liu, J., Tian, C., Jiang, T., Ricohermoso, E. I., Yu, Z., Ionescu, E., ... & Riedel, R. (2023). Polymer-derived SiOC ceramics: a potential catalyst support controlled by the sintering temperature and carbon content. *Journal of the European Ceramic Society*, *43*(8), 3191-3200. https://doi.org/10.1016/j.jeurceramsoc.2023.02.045

[3] Sun, W., Zhou, H., Tan, X., Wang, K., Ruan, H., Zhang, H., ... & Chen, X. (2018). Adjustable microwave dielectric properties of ZnO–TiO2–ZrO2–Nb2O5 composite ceramics via controlling the raw ZrO2 content and sintering temperature. *Journal of Materials Science: Materials in Electronics*, *29*(14), 12055-12060. https://doi.org/10.1007/s10854-018-9311-x

[4] Chi, Z., Chen, X., Xia, H., Liu, C., & Wang, Z. (2024). An adaptive control system based on spatial–temporal graph convolutional and disentangled baseline-volatility prediction of bellows temperature for iron ore sintering process. *Journal of Process Control*, *140*, 103254. https://doi.org/10.1016/j.jprocont.2024.103254

[5] Fan, W., Peng, Z., Yin, T., Xiang, C., Tang, H., Ye, L., & Rao, M. (2024). Tailoring tactics for preparation of superior thermal insulation materials from blast furnace ferronickel slag: Control of sintering temperature. *Process Safety and Environmental Protection*, *186*, 1242-1252. https://doi.org/10.1016/j.psep.2024.04.041

[6] Erkınay Özdemir, M., Beşkardeş, A., & Hameş, Y. (2024). Intelligent sinter machine speed control system using optimized fuzzy logic controller: An experimental study in iron and steel plant. *Arabian Journal for Science and Engineering*, *49*(12), 16391-16406. https://doi.org/10.1007/s13369-024-08981-z

[7] Li, L., Wang, S., Chen, L., Hou, H., & Zhao, Y. (2024). Improved corrosion resistance of AZ91D through sintering temperature control for second phase precipitation. *Materials Characterization*, *209*, 113690. https://doi.org/10.1016/j.matchar.2024.113690

[8] Wang, H. J., & Bian, J. J. (2024). Tuning the temperature coefficient of the resonant frequency of the AlPO4–BPO4–SiO2 ternaries with TiO2 addition and sintering atmosphere control. *Journal of the European Ceramic Society*, *44*(4), 2144-2149. https://doi.org/10.1016/j.jeurceramsoc.2023.10.031

[9] Choi, S. J., Jang, J. S., Park, H. J., & Kim, I. D. (2017). Optically sintered 2D RuO2 nanosheets: temperature-controlled NO2 reaction. *Advanced Functional Materials*, *27*(13), 1606026. https://doi.org/10.1002/adfm.201606026

[10] Bulat, L., Novotel'nova, A., Tukmakova, A., Yerezhep, D., Osvenskii, V., Sorokin, A., ... & Ashmontas, S. (2017). Temperature fields control in the process of spark plasma sintering of thermoelectrics. *Technical Physics*, *62*(4). https://doi.org/10.1134/S1063784217040053

[11] Giuntini, D., Chen, I. W., & Olevsky, E. A. (2016). Sintering shape distortions controlled by interface roughness in powder composites. *Scripta Materialia*, *124*, 38-41. https://doi.org/10.1016/j.scriptamat.2016.06.024

[12] Lu, G., Chen, J. L., Yan, Q. S., Tu, Z. X., & Chen, Y. S. (2025). Zero-shrinkage densification of Y_2O_3-based ceramic cores via in-situ Al reaction and sintering temperature control. *Ceramics International*, *51*(24PA), 40719–40734. https://doi.org/10.1016/j.ceramint.2025.06.319

[13] Dai, Y., Chen, N., & Shao, Z. (2025). Hybrid self-learning model for the prediction and control of sintering furnace temperature. *Control Engineering Practice*, *154*, 106159. https://doi.org/10.1016/j.conengprac.2024.106159

[14] Abdelrahman, M., & Starr, T. L. (2016). Quality certification and control of polymer laser sintering: layerwise temperature monitoring using thermal imaging. *The International Journal of Advanced Manufacturing Technology*, *84*(5), 831-842. https://doi.org/10.1007/s00170-015-7524-1

[15] Garrigues, A. R., Wang, L., Del Barco, E., & Nijhuis, C. A. (2016). Electrostatic control over temperature-dependent tunnelling across a single-molecule junction. *Nature communications*, *7*(1), 11595. https://doi.org/10.1038/ncomms11595

[16] Voisin, T., Durand, L., Karnatak, N., Le Gallet, S., Thomas, M., Le Berre, Y., ... & Couret, A. (2013). Temperature control during Spark Plasma Sintering and application to up-scaling and complex shaping. *Journal of Materials Processing Technology*, *213*(2), 269-278. https://doi.org/10.1016/j.jmatprotec.2012.09.023

[17] Molénat, G., Durand, L., Galy, J., & Couret, A. (2010). Temperature control in Spark Plasma sintering: an FEM approach. *Journal of Metallurgy*, *2010*(1), 145431. https://doi.org/10.1155/2010/145431

[18] Morel, C., & Morel, J. Y. (2025, April). Chaos Anticontrol and Switching Frequency Impact on MOSFET Junction Temperature and Lifetime. In *Actuators* (Vol. 14, No. 5, p. 203). MDPI. https://doi.org/10.3390/act14050203

[19] Chen, C., Yin, S., Liu, J., Sun, C., Zhang, Y., Liu, L., & Zuo, R. (2026). High-Strength, High-Thermal-Conductivity Si3N4 Ceramics via Synergistic Slurry and Sintering Control. *Ceramics International*. https://doi.org/10.1016/j.ceramint.2026.04.190

[20] Chen, J., Gui, W., Chen, N., Peng, W., Liu, R., Zhou, X., ... & Guo, Y. (2025). An Energy-Efficient Sintering Temperature Multimode Control and Optimization for High-Quality Ternary Cathode Materials. *Future Batteries*, *5*, 100034. https://doi.org/10.1016/j.fub.2025.100034

[21] Mora-Barzaga, G., Inostroza, P., Valencia, F., & Bringa, E. (2026). Ultrafast thermal sintering controls thermal transport in high-entropy alloy nanoparticle junctions. *International Journal of Heat and Mass Transfer*, *270*, 129207. https://doi.org/10.1016/j.ijheatmasstransfer.2026.129207

[22] Chen, J., Gui, W., Chen, N., Li, H. X., Luo, B., & Li, B. (2026). Self-Triggered H∞ temperature field control for the time-delay sintering process of cathode materials via adaptive dynamic programming. *Control Engineering Practice*, *176*, 107142. https://doi.org/10.1016/j.conengprac.2026.107142

[23] Kang, L., Qi, A., Dong, H., Fan, W., Zhang, Z., Jiang, X., & Liu, G. (2026). Boron carbide for HTGR control rods: Sintering, temperature-dependent properties, and thermal shock resistance. *International Journal of Applied Ceramic Technology*, *23*(1), e70140. https://doi.org/10.1111/ijac.70140

[24] Li, B., Cao, X., Luo, B., Gao, J., Chen, N., Chen, J., ... & Gui, W. (2025). Asymmetric ADP-driven event-triggered optimal control of industrial sintering temperature field with input constraints. *Neurocomputing*, 131877. https://doi.org/10.1016/j.neucom.2025.131877

[25] Liu, H., Zhao, X., Xu, J., Xia, W., Yue, Q., Yuan, Y., ... & Zhang, Z. (2026). A Strategy for Intermediate-temperature Plasticity Control in Polycrystalline Alloys Based on Equal-Cohesive Temperature. *Materials Science and Engineering: A*, 150454. https://doi.org/10.1016/j.msea.2026.150454

APA Citation

He, Y., & Yang, J. (2026). Research on Sintering End Temperature Control Based on Fuzzy Adaptive PID Control. *International Scientific Technical and Economic Research, 4(3),* 44-59. **https://doi.org/10.67541/ISTAER2625**